ARL-TR-8628 ● JAN 2019

US Army Research Laboratory

Development of a Computational Framework to Study Ion Transport through Mechanosensitive Ion Channels

by Robert M Elder, Yelena R Sliozberg, and Tanya L Chantawansri

NOTICES

Disclaimers

The findings in this report are not to be construed as an official Department of the Army position unless so designated by other authorized documents.

Citation of manufacturer's or trade names does not constitute an official endorsement or approval of the use thereof.

Destroy this report when it is no longer needed. Do not return it to the originator.

ARL-TR-8628 ● JAN 2019

US Army Research Laboratory

Development of a Computational Framework to Study Ion Transport through Mechanosensitive Ion Channels

by Robert M Elder
Bennett Aerospace, Inc., Cary, NC

Yelena R Sliozberg
SURVICE Engineering Company, Belcamp, MD

Tanya L Chantawansri
Vehicle Technology Directorate, ARL

REPORT DOCUMENTATION PAGE

Form Approved
OMB No. 0704-0188

1. REPORT DATE *(DD-MM-YYYY)*	2. REPORT TYPE	3. DATES COVERED (From - To)
January 2019	Technical Report	April 2016 to December 2018

4. TITLE AND SUBTITLE
Development of a Computational Framework to Study Ion Transport through Mechanosensitive Ion Channels

5a. CONTRACT NUMBER

5b. GRANT NUMBER

5c. PROGRAM ELEMENT NUMBER

6. AUTHOR(S)
Robert M Elder, Yelena R Sliozberg, and Tanya L Chantawansri

5d. PROJECT NUMBER

5e. TASK NUMBER

5f. WORK UNIT NUMBER

7. PERFORMING ORGANIZATION NAME(S) AND ADDRESS(ES)
US Army Research Laboratory
ATTN: RDRL-VT
Aberdeen Proving Ground, MD 21005

8. PERFORMING ORGANIZATION REPORT NUMBER
ARL-TR-8628

9. SPONSORING/MONITORING AGENCY NAME(S) AND ADDRESS(ES)

10. SPONSOR/MONITOR'S ACRONYM(S)

11. SPONSOR/MONITOR'S REPORT NUMBER(S)

12. DISTRIBUTION/AVAILABILITY STATEMENT
Approved for public release; distribution is unlimited.

13. SUPPLEMENTARY NOTES
ORCIDs: Elder, 0000-0002-5052-3841; Chantawansri, 0000-0003-0377-3116

14. ABSTRACT
External physical forces on neurons can alter cell-membrane tension and activate mechanosensitivity in ion channels, thereby altering membrane electrostatic potential, which may exacerbate traumatic brain injury. We present an efficient computational framework for studying ion channels under user-specified conditions of membrane potential, membrane tension, and asymmetric concentrations of multiple ion species. We demonstrate the use of the framework on a model neuronal K^+ ion channel, finding reasonable agreement with experimental results. The methodology is general and can be applied to other ion channels and membrane proteins with various combinations of membrane potential, membrane tension, and ion concentration gradient.

15. SUBJECT TERMS
mechanosensitive ion channel, molecular dynamics, ion transport, TWIK-related arachidonic acid-stimulated K^+ channel, TRAAK

16. SECURITY CLASSIFICATION OF:			17. LIMITATION OF ABSTRACT	18. NUMBER OF PAGES	19a. NAME OF RESPONSIBLE PERSON
a. REPORT	b. ABSTRACT	c. THIS PAGE			Tanya Chantawansri
Unclassified	Unclassified	Unclassified	UU	25	19b. TELEPHONE NUMBER (Include area code) (410) 278-3760

Standard Form 298 (Rev. 8/98)
Prescribed by ANSI Std. Z39.18

Contents

List of Figures

List of Tables

Acknowledgments

The authors thank Dr T Weerasooriya and Dr AM Dileonardi of the US Army Research Laboratory (ARL) for useful discussions, and we thank ARL Technical Editor Martin Kufus for a close reading of the manuscript. This work was supported by grants of computing time from the Department of Defense High Performance Computing Modernization Program. The research reported in this document was performed in connection with Contract W911QX-16-D-0014 with ARL. The views and conclusions contained in this document are those of Bennett Aerospace, Inc., and ARL. The US Government is authorized to reproduce and distribute reprints for Government purposes notwithstanding any copyright notation hereon.

1. Introduction

Regulation of both the intra- and extracellular concentration of ions (ion homeostasis) mediated by ion channels is a process of fundamental importance and constitutes a necessary condition to sustain life. Changes to ion homeostasis can result from a cascade of events that are initiated by mechanical strain resultant from an external physical force and contributes to cell damage and death in traumatic brain injury (TBI). Because TBI is caused by a physical insult, ions can enter through transient neuronal membrane pores formed by tear–shearing forces during the primary injury.[1–4] However, membrane poration only accounts for a portion of injured neurons.[5] The evidence suggests that—in addition to producing pores in cell membranes—mechanical strain by the external physical force can cause disturbances to existing membrane proteins and mechanically activate some mechanosensitive intracellular structures.[6–8] For instance, voltage-gated Na^+ channels and *N*-methyl-D-aspartate receptors are known to be sensitive to the mechanical stress that can occur during mild TBI.[9,10]

Another example from the many mechanosensitive ion channels found in the brain is TWIK-related arachidonic acid-stimulated K^+ channel (TRAAK), which is expressed predominantly in the nervous system.[11,12] TRAAK belongs to the well-studied subfamily of two-pore domain K^+ (K2P) ion channels. K2P channels are dimers formed from two polypeptide chains (subunits), which make up the ion-conducting channel. Experimental research shows that K2P channels control the resting potential in many cells.

The mechanosensitivity of the TRAAK channel is mediated directly through a lipid membrane; that is, mechanical force from the lipid membrane places TRAAK in a conductive state. For example, lateral membrane tension can control channel gating.[13] TRAAK is activated by a broad variety of mechanical forces, which can be applied to cells by stretching, poking, swelling, or fluid jet stimulation, or to excised membrane patches through pressure-induced stretch.[14] Recent studies demonstrate the sensitivity of TRAAK channel to mechanical perturbations of the cell membrane using electrophysiological recordings.[13,15]

In the absence of significant membrane tension, the TRAAK channel has a low (~1%) open probability, which may serve as background current to set and stabilize the resting membrane potential.[14] TRAAK is further activated under relatively low tension values of an unpressurized patch (0.5–4.0 mN/m), which is caused by the adhesion of lipids to the glass pipette.[13,15] Activation increases with increasing tension created by pressurizing and stretching membrane patches up to lytic values

(~12 mN/m). Thus, TRAAK has a low threshold for tension activation and is activated over the entire range of tension a membrane can withstand.[14]

TRAAK exists in two distinct conformations, termed open (conductive) and closed (nonconductive).[13] In the open state, the ionic conduction pathway through the channel is unobstructed from the intracellular cytoplasm to the extracellular environment. In the closed state, two transmembrane helices shift slightly, thereby opening fenestrations (windows) in the intracellular cavity that precedes the selectivity filter (SF). The cavity is exposed to the surrounding lipid bilayer through the fenestrations, which allow lipid acyl chains to enter the cavity and block ion conduction. The open conformation is sealed from the surrounding membrane, which prevents lipid block and permits ion conduction.[14] Similar fenestrations have been noted in other K2P channels. These fenestrations are hypothesized to allow the entry of lipids and other hydrophobic molecules into the conduction path,[16] and in fact lipids have been directly observed in this role experimentally[17] and in simulations.[18] Thus, this mechanism is important for a large class of medically relevant ion channels. Two conformational changes are predicted to underlie TRAAK mechanosensitivity: area expansion and the flattening of the channel surface in the membrane upon opening. Membrane tension favors protein expansion.[19] The wider and flatter TRAAK conformations are conductive because these conformations seal the fenestrations that allow lipids to block ion conduction.[14] We note, however, that recent work with a similar protein (TREK-2, also in the K2P subfamily) casts doubt that a direct lipid block is the primary mechanism of mechano-gating.[20]

Our primary goal in this work is to develop a framework using molecular dynamics (MD) to apply mechanical loading to an ion channel embedded in a lipid membrane with asymmetric ion concentrations across the membrane. This framework can be used to understand the influence of membrane stretch, ion concentration, and other factors on conduction through the channel. As an example of applying this framework, we use the TRAAK channel in both the open and closed states (Fig. 1). Various degrees of deformation and membrane potential represented by a constant electric field are examined. We present results that exemplify the types of output that can be expected from the framework.

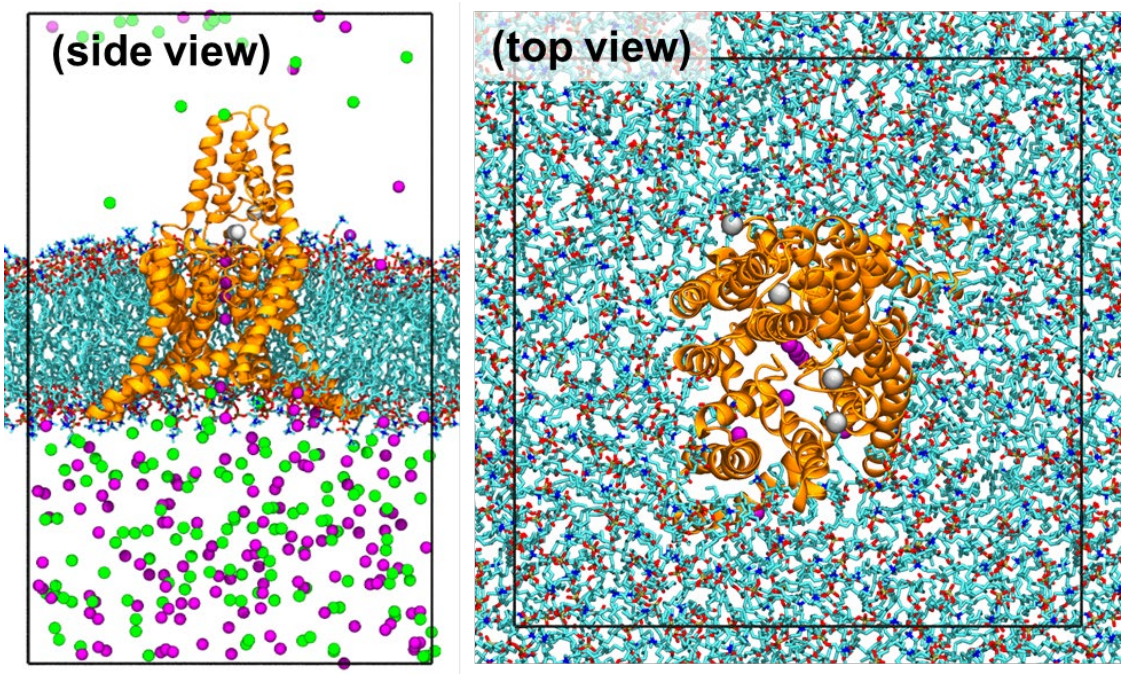

Fig. 1 Side and top views of the TRAAK protein embedded in a POPC lipid bilayer. The protein is represented as orange ribbons. Ions are shown as spheres colored by element: potassium, purple; chloride, green; and calcium, gray. The boundaries of the simulation box are shown as black lines. Periodic images of the lipid bilayer (licorice representation and colored by element) are shown. Water molecules and hydrogen atoms are hidden for clarity.

2. Methods

Systems studied and conditions simulated. We studied the TRAAK protein in the open and closed states embedded in a lipid bilayer. We maintained a 10:1-concentration K^+ gradient across the membrane, mimicking the physiological difference between the intra- and extracellular environments[21] and similar to recent experimental studies.[14,17] For both TRAAK structures, we simulated the protein with or without 10-mN/m membrane tension and with or without an applied 150-mV electric field, for a total of eight simulations under different conditions. We note that the highest membrane tension applied (10 mN/m) is just below typical values that cause cell lysis (~12 mN/m). The following subsections describe the computational framework we developed for studying these types of systems and conditions.

System construction. We began with the crystal structures of the TRAAK protein in the open and closed states (Protein Data Bank [PDB] codes 4WFE and 4WFF, respectively). The PDB structures were modified in the following ways to prepare them for simulations. The antibody chains bound to the TRAAK protein were discarded. The PDB structures are missing short segments of two flexible loops.[17] We inserted these missing residues using Discovery Studio with the random tweak

algorithm of Shenkin et al.,[22] and the loop conformations were relaxed using energy minimization with the remainder of the protein coordinates constrained. In the crystal structure, two Ca^{2+} atoms are bound near the flexible loop in Subunit A but not in Subunit B. By virtue of the bilateral symmetry of K2P channels, we placed two Ca^{2+} atoms in similar locations in Subunit B. All of the Ca^{2+} ions remained stably bound by the loops throughout all simulations. The lipid block in the closed structure was modeled as a short, aliphatic molecule (decane), which was the only portion of the block that was resolved in the experimental structure; including one or more full lipid molecules in the block is an interesting topic for future work. These optimized protein structures were inserted into a lipid bilayer consisting of POPC (palmitoyl-oleoyl-phosphatidyl-choline) molecules, constructed using the Visual Molecular Dynamics (VMD) Membrane Builder,[23] with the central channel axis and the bilayer normal aligned in the *z* dimension. POPC lipids are similar to the phosphatidylcholine lipid mixture used in Brohawn et al.[17] Lipids within 5 Å of the protein were deleted, leaving about 250 lipid molecules in the bilayer. The protein-membrane system was solvated approximately 40,000 water molecules, and 146 K^+ and 142 Cl^- ions were added to neutralize the charge and bring the ion concentration to approximately 150 mM. The total number of atoms was approximately 150,000.

Equilibration procedure. We equilibrated the system with the following procedure. First, with the protein and Ca^{2+} atoms restrained with 10-kcal/(mol-Å^2) harmonic restraints, we conducted 10,000 steps of conjugate gradient energy minimization, 0.8 ns of constant volume–constant temperature (NVT) MD, and 0.8 ns of constant pressure–constant temperature (NPT) MD to equilibrate water, lipids, and K^+ and Cl^- ions. No surface tension was applied until later in the equilibration process. Next, with the restraints on the protein removed but with Ca^{2+} still restrained by 1-kcal/(mol-Å^2) harmonic restraints, we conducted 60 ns of NPT MD. Then, the restraints on Ca^{2+} were eliminated, we conducted another 60 ns of NPT MD. During this last step, and during all subsequent simulations, we used the *collective variables* module[24] of Nanoscale Molecular Dynamics (NAMD) to restrain (harmonic spring constant 10 kcal/mol-Å^2) the center-of-mass of the protein selectivity filter to the center of the simulation box to prevent translational drift.

We established an asymmetric ion concentration by taking the equilibrated structure and manually placing the K^+ and Cl^- ions such that the concentrations were approximately 30 mM and approximately 300 mM above and below the membrane, respectively. Thus, the regions above (+*z*) and below (–*z*) the membrane model the extracellular and intracellular environments, respectively. Then, we maintained the asymmetric concentration using the method of Roux and coworkers[25] where forces are applied to K^+ ions in a small boundary layer between

the two regions of differing concentration. We used a layer width of 5.0 Å, and the force was dynamically adjusted to achieve the target 10:1 concentration ratio (using smoothing parameters of $\tau = 1000$ and $\alpha = 100$ in Eq. 15 of Khalili-Araghi et al.[25]). This method for maintaining asymmetric ion concentrations has a lower computational cost than other methods, such as a double-membrane system.[25,26] We also note that this method can be applied simultaneously to multiple ionic species, such as K^+, Na^+, Cl^-, and Ca^{2+}, and could be extended to create time-dependent concentration changes. We conducted another 200-ns NPT MD, still without applied surface tension, to ensure the concentration gradient and structure were equilibrated. Finally, we equilibrated the systems for another 100 ns with the surface tension set to zero or 10 mN/m. The final simulation box dimensions were approximately (98, 98, 159) Å in the (x, y, z) dimensions with zero surface tension and approximately (99, 99, 158) Å with 10-mN/m tension.

Simulation protocol. Using the equilibrated structures, we conducted production simulations for 1.0 μs using NVT MD with either zero or 150-mV electric field aligned in the $+z$ direction; that is, from intracellular to extracellular. The strength of the applied electric field was calculated using the length of the simulation box rather than the membrane thickness.[27] An applied electric field is equivalent to a transmembrane potential created by ion concentration gradients.[27]

A Langevin thermostat and barostat were used to control the temperature (damping coefficient of 1 ps^{-1}) and pressure (piston period of 100 fs and piston-decay constant of 50 fs) at 300 K and 1 atm. The simulation cell was periodic in all three dimensions. The cell dimensions were allowed to vary independently, except that the ratio of the x and y box dimensions was maintained as unity. The Shake and Settle algorithms were used to constrain bonds involving hydrogen,[28,29] and a time step of 2 fs was used. Long-range electrostatic interactions were treated with the particle-mesh Ewald (PME) method,[28] with a tolerance of 10^{-6} and interpolation order of 4. The reversible reference system propagator algorithm (RESPA) integration scheme was used,[30] with short-range forces calculated every time step and long-range forces calculated every other time step. The short-range nonbonded cutoff was 10 Å with a switching function between 8 and 10 Å, and the pairwise neighbor list was updated every 20 time steps. Atomic coordinates were recorded every 20 ps. The Amber *ff14SB* and *lipid14* force fields were used for protein and lipids, respectively. Water was described with the transferable intermolecular potential with 3 points (TIP3P) force field,[31] and ions were modeled using force fields optimized for use with PME and TIP3P water.[32,33] The general Amber force field was used for the decane molecule that served as a lipid block in the closed state.[34–37] The program NAMD Version 2.10 was used for all simulations.[38]

Analytical methods. We quantified ion conduction by monitoring the cumulative number of ion permeation events (i.e., how many ions have passed through the channel). An ion permeation event was defined to occur when an ion initially in the intracellular region (below the membrane, Fig. 1) entered the channel—specifically, approached to within 7 Å of the center-of-mass of the selectivity filter—and then exited into the extracellular region (above the membrane, Fig. 1). If the ion instead exited the SF back into the intracellular region, no permeation event was counted. We also checked for permeation events in the opposite direction, as well as water or Cl^- permeation events, but none occurred. The 7-Å cutoff encompasses ions located at the ion-binding sites of the selectivity filter. Additionally, we quantified the radius of the channel along the *z*-dimension, which is aligned with the membrane normal and the protein conduction path. To this end, at several increments of *z* separated by 0.5 Å and aligned with the (*x*,*y*) coordinates of the center-of-mass of the SF, we calculated the largest sphere that could be inserted without overlapping any protein atoms; the radius of the channel was defined as the radius of this sphere. VMD was used for analysis and visualization.[23]

3. Results

First, we consider K^+ ion conduction through the TRAAK channel in the open conformation under the various conditions of tension of electric field. We quantify ion conduction using the cumulative number of ion permeation events (Fig. 2). The slope of a linear fit to the number of permeation events versus time is the electrical current through the channel, which is given in Table 1 for all conditions studied here. With zero applied field the current is approximately 4–5 pA, while with a 150-mV field the current rises to approximately 11–12 pA. Thus, our simulations capture the expected increase in current with applied voltage. Furthermore, the conductance, *G*, of the ion channel is calculated as $\Delta I/\Delta V$, where ΔI is the change in current that occurs with ΔV, the change in voltage (i.e., the slope of a linear current–voltage plot[39–41]). The change in current of approximately 7 pA with the change in voltage of 150 mV corresponds to a conductance of about 47 pS. This value is in good agreement with single-channel experimental values of TRAAK, which are around 50 pS under roughly similar conditions.[39,42] This level of agreement is comparable to previous simulation studies.[41] Additionally, we estimate the reversal potential for this system—the applied field at which the current would become zero—by linearly extrapolating from the current-versus-field data. This gives a K^+ membrane potential of around –70 to –130 mV, depending on the conditions, which is reasonably close to experimental values (roughly –60 mV).[13] However, the conditions for that measurement were quite different from the simulations described here: The

experiments measured the whole-cell current response of TRAAK-expressing Chinese hamster ovary cells under voltage clamp while applying pressure with a glass slide.[13] Hence, multiple proteins and ionic species are present in the experiments, and perfect agreement between experiments and simulations cannot be expected. Overall, the effect of applied electric fields—equivalent to the membrane electrostatic potential—is correctly captured within our computational framework.

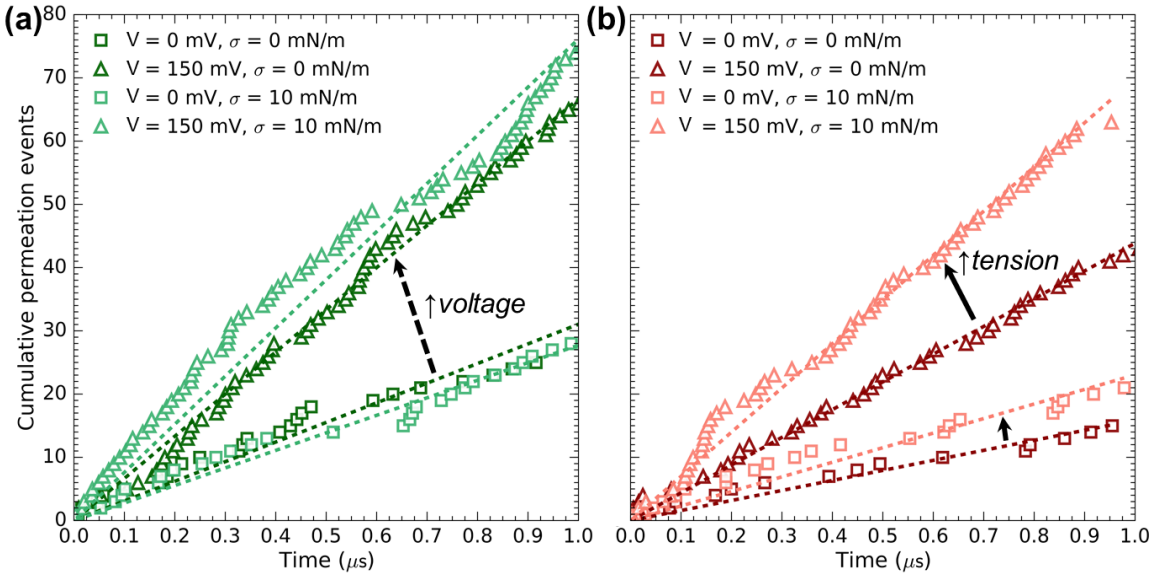

Fig. 2 Ion conduction through the TRAAK channel in the a) open and b) closed conformations. The applied electric field, V, is either zero or 150 mV. The membrane surface tension, σ, is either zero or 10 mN/m. Each data point represents a discrete ion permeation event at the indicated time. Dashed lines are linear fits. The dashed arrow indicates the effect of increasing voltage, while the solid arrows indicate the effect of increasing membrane tension.

Table 1 Electrical properties of TRAAK under various conditions; current is given as mean ± standard error from linear fit to cumulative permeation events vs. time

Protein structure	Electric field, V (mV)	Tension, σ (mN/m)	Current (pA)	Conductance (pS)	Reversal potential (mV)
Open	0	0	5.0 ± 0.7	…	…
Open	0	10	4.4 ± 0.4	…	…
Open	150	0	10.7 ± 0.4	38	–132
Open	150	10	12.2 ± 1.2	52	–85
Closed	0	0	2.5 ± 0.3	…	…
Closed	0	10	3.7 ± 0.6	…	…
Closed	150	0	7.0 ± 0.3	30	–74
Closed	150	10	11.2 ± 0.6	50	–83

Note: Conductance and reversal potential are shown in rows where V = 150 mV, although these data are derived from simulations using zero and 150-mV applied field.

Interestingly, for the open state of TRAAK there is no effect of membrane tension on ion flux. The reason for this may be that the open state is already fully conductive, because the channel is not occluded by a lipid tail extending from the membrane. It is possible that, given enough time, in the absence of membrane tension the initial open conformation would transition to a closed conformation, with open fenestrations and lipids blocking the channel. However, such a transition is likely beyond the reach of typical MD simulations, which are currently limited to the microsecond time scale.

Next, we examine ion conduction in the closed state of TRAAK, where the ion conduction path is at least partially occluded by a lipid-like molecule in the intracellular cavity. The number of permeation events versus time (Fig. 2b) demonstrates three interesting trends, which are more easily perceived through the current (Table 1). First, applying an electric field has the expected effect of increasing the current (e.g., 2.1 pA vs. 6.7 pA as V increases from 0 to 150 mV, with σ = 0 mN/m). Second, compared to the open state, the current is weaker in the closed state in the absence of tension (e.g., 10.8 pA vs. 6.7 pA, with V = 150 mV and σ = 0 mN/m). Third, and most interesting, applying membrane tension to the closed state restores its conductivity to that of the open state (e.g., 10.8 pA vs. 10.6 pA, with V = 150 mV and σ = 10 mN/m). Thus, our framework is able to qualitatively demonstrate the expected mechanosensitivity of the TRAAK ion channel.[13,15] Quantitatively, however, the conductivity in the closed state is not as low as would be expected based on experiments, where it is approximately 1% of the open state.[14] We suggest this discrepancy arises because the "lipid" block in our

simulations is only a single small aliphatic molecule (decane), not multiple full-sized lipid molecules with connections to the membrane, which could block the channel more effectively.

One of the primary benefits of using atomically detailed molecular simulations is the molecular-level insight that can be gleaned, which is difficult or impossible to obtain by other means. As a demonstration, to elucidate how tension restores conductivity to the closed state, we characterized the radius of the ion channel pore under various conditions (Fig. 3). First we describe these data in qualitative terms. Starting from the intracellular side (z = –30 Å), the pore is rather large (~10 Å). Traveling in the positive *z*-direction, the pore shrinks before widening into an intracellular cavity (IC) at z ≈ –20 Å. This IC is the location of the lipid block in the closed conformation. Then the pore again contracts as the SF begins, where we find an undulating pattern with four small peaks at which ions reside while transiting the SF (z ≈ 0 Å). Finally, the pore widens on the extracellular side (z ≈ 10 Å).

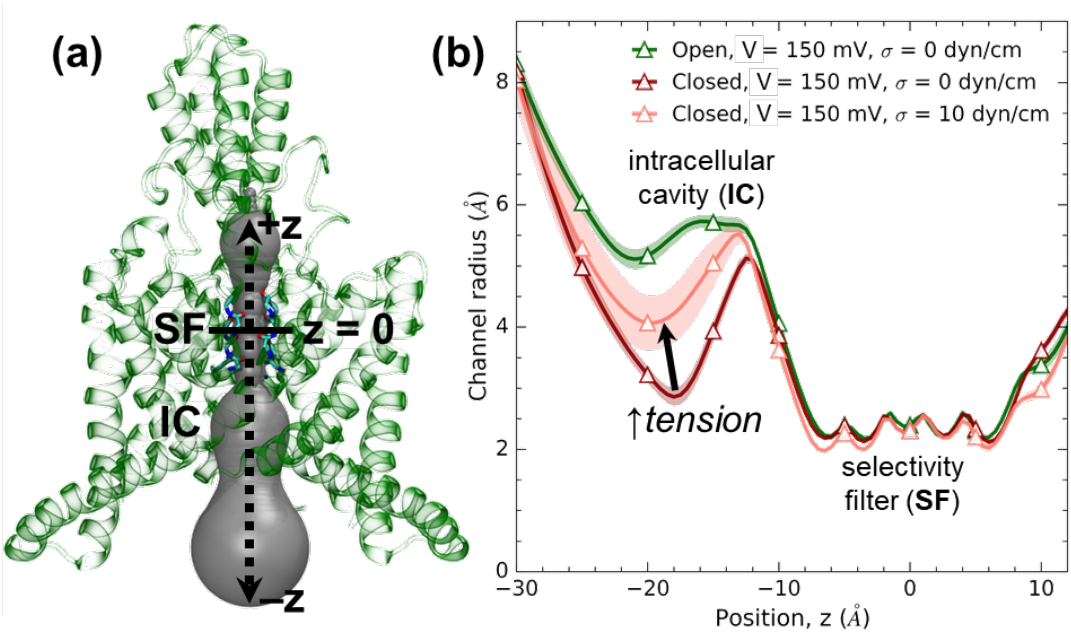

Fig. 3 Radius of the ion-conducting pore in TRAAK. The SF is centered on z = 0 Å. The intracellular side is in the negative *z*-direction, while the extracellular side is in the positive *z*-direction. An IC at z ≈ -14 Å is separated from the intracellular fluid by a slight constriction of the pore (z ≈ -20 Å).

In more quantitative terms, the key observation is that the amount of contraction preceding the IC depends on the protein conformation and conditions. There is very little contraction in the open state, with the IC remaining at 5–6 Å, whereas in the closed state the pore radius drops to approximately 3 Å in the absence of membrane

tension (Fig. 3b). Notably, the hydrodynamic radius of the K^+ ion (i.e., the size of the ion including bound water molecules) is around 3.5–4 Å.[43,44] To pass through the channel, the ion must shed these bound waters, and the ion–water interactions must be replaced by other interactions. In the absence of tension in the closed state, this hydrodynamic radius is larger than the pore radius at the entrance to IC, suggesting that K^+ ions are partially excluded based on size. Thus, one plausible explanation for how membrane tension restores conductivity to the closed state is by expanding the intracellular cavity entrance to approximately 4 Å, thereby allowing hydrated K^+ ions to progress through the channel. (The SF, although smaller than 4 Å, provides specific interactions that effectively replace the hydration shell.) This finding that membrane tension increases the area of the protein is consistent with previous studies.[17] However, we note that this is only a cursory glance at what is undoubtedly a complicated mechanism of mechano-gating, which likely involves multiple subtle conformational shifts.[20,45]

4. Conclusions

We developed a computational framework for studying membrane proteins, such as ion channels, with user-specified membrane potential, membrane surface tension, and asymmetric ion concentrations. Although other groups have used similar methods previously (e.g., the study of stretch-induced conformational changes in another K2P channel in Aryal et al.[20]), to the best of our knowledge we are the first to bring this set of tools together comprehensively. The framework could be used to study, for example, changes to neuronal ion homeostasis in response to external physical forces that occur in mild TBI, or the response of voltage-gated ion channels to changes in ionic strength or voltage. As an example, we applied the framework to an important neuronal ion channel, TRAAK, to demonstrate that this methodology can accurately capture experimental results. We emphasize that this framework is not limited to the conditions employed here: It is designed to apply to any ion channel with an available experimental structure, any lipid composition, any membrane potential, any membrane surface tension (or even compression), and any ion composition and gradient, including time-dependent gradients. Furthermore, we demonstrated some of the types of useful mechanistic insight that can be gained by examining the atomic-level details of molecular simulations.

We briefly comment on the computational expense of these simulations. Each of the eight conditions required a 1-μs simulation, each of which required over 1 month of straight computation using 288 processors on a modern supercomputer. Thus, each simulation required approximately 300,000 CPU-hours, for a total of approximately 2,400,000 CPU-hours for this study. While this expense is not

unreasonable on current hardware, it is still considerable. If it were necessary to study numerous proteins or other numerous conditions, or to conduct replicate simulations under the same conditions to improve statistical sampling, the expense could quickly mushroom into infeasibility. Thus, in the absence of specialized hardware designed to accelerate such simulations,[46] we suggest that future extensions of the framework should include enhanced sampling methods to accelerate ion flux,[47,48] thereby reducing the computational expense.

5. References

1. LaPlaca MC, Prado GR, Cullen DK, Irons HR. High rate shear insult delivered to cortical neurons produces heterogeneous membrane permeability alterations. 28th Annual International Conference of the IEEE Engineering in medicine and biology society; 2006; EMBS; c2006. p. 2385–2387.

2. Cullen DK, Vernekar VN, LaPlaca MC. Trauma-induced plasmalemma disruptions in three-dimensional neural cultures are dependent on strain modality and rate. J Neurotr. 2011;28:2219–2233.

3. Arun P, Abu-Taleb R, Valiyaveettil M, Wang Y, Long JB, Nambiar MP. Transient changes in neuronal cell membrane permeability after blast exposure. Neuroreport. 2012;23:342–346.

4. Arun P, Abu-Taleb R, Oguntayo S, Tanaka M, Wang Y, Valiyaveettil M, Long JB, Zhang Y, Nambiar P. Distinct patterns of expression of traumatic brain injury biomarkers after blast exposure: role of compromised cell membrane integrity. Neurosci Lett. 2013;552:87–91.

5. Hemphill MA, Dabiri BE, Gabriele S, Kerscher L, Franck C, Goss JA, Alford PW, Parker KK. A possible role for integrin signaling in diffuse axonal injury. PLoS ONE. 2011;6:1–11.

6. Taylor WJ. The mechanobiology of brain function. Nat Rev Neurosci. 2012;13:867–878.

7. Hemphill MA, Dauth S, Yu CJ, Dabiri BE, Parker KK. Traumatic brain injury and the neuronal microenvironment: a potential role for neuropathological mechanotransduction. Neuron. 2015;85:1177–1192.

8. Maneshi MM, Sachs F, Hua SZ. A threshold shear force for calcium influx in an astrocyte model of traumatic brain injury. J Neurotrama. 2015;32:1020–1029.

9. Weber J. Altered calcium signaling following traumatic brain injury. Front Pharmacol. 2012;3;1–16.

10. Hinzman JM, Thomas TC, Burmeister JJ, Quintero JE, Huettl P, Pomerleau F, Gerhardt GA, Lifshitz J. Diffuse brain injury elevates tonic glutamate levels and potassium-evoked glutamate release in discrete brain regions at two days post-injury: an enzyme-based microelectrode array study. J Neurotr. 2010;27:889–899.

11. Brohawn SG, del Marmol J, MacKinnon R. Crystal structure of the human K2P TRAAK, a lipid- and mechano-sensitive K+ ion channel. Science. 2012;335:436–441.

12. Brohawn SG, Campbell EB, MacKinnon R. Domain-swapped chain connectivity and gated membrane access in a Fab-mediated crystal of the human TRAAK K+ channel. Proc Natl Acad Sci USA. 2013;110:2129–2134.

13. Brohawn SG, Su Z, MacKinnon R. Mechanosensitivity is mediated directly by the lipid membrane in TRAAK and TREK1 K+ channels. Proc Natl Acad Sci USA. 2014;111:3614–3619.

14. Brohawn SG. How ion channels sense mechanical force: insights from mechanosensitive K2P channels TRAAK, TREK1, and TREK2. Ann NY Acad Sci. 2015;1352:20–32.

15. Schmidt D, del Marmol J, MacKinnon R. Mechanistic basis for low threshold mechanosensitivity in voltage-dependent K+ channels. Proc Natl Acad Sci USA. 2012;109:10352–10357.

16. Braun AP. Two-pore domain potassium channels: variation on a structural theme. Channels. 2012;6:139–140.

17. Brohawn SG, Campbell EB, MacKinnon R. Physical mechanism for gating and mechanosensitivity of the human TRAAK K+ channel. Nature. 2014;516:126–130.

18. Jorgensen C, Darré L, Oakes V, Torella R, Pryde D, Domene C. Lateral fenestrations in K+-channels explored using molecular dynamics simulations. Mol Pharm. 2016;13:2263–2273.

19. Phillips R, Ursell T, Wiggins P, Sens P. Emerging roles for lipids in shaping membrane-protein function. Nature. 2009;459:379–385.

20. Aryal P, Jarerattanachat V, Clausen MV, Schewe M, McClenaghan C, Argent L, Conrad LJ, Dong YY, Pike ACW, Carpenter EP, Baukrowitz T, Sansom MSP, Tucker SJ. Bilayer-mediated structural transitions control mechanosensitivity of the TREK-2 K2P channel. Structure. 2017;25:708–718.

21. Furini S, Domene C. K+ and Na+ Conduction in Selective and Nonselective Ion Channels Via Molecular Dynamics Simulations. Biophys J. 2013;105:1737–1745.

22. Shenkin PS, Yarmush DL, Fine RM, Wang H, Levinthal C. Predicting antibody hypervariable loop conformation. I. Ensembles of random conformations for ringlike structures. Biopolymers. 1987;26:2053–2085.

23. Humphrey W, Dalke A, Schulten K. VMD: visual molecular dynamics. J Mol Graphics. 1996;14:33–38.

24. Fiorin G, Klein ML, Hénin J. Using collective variables to drive molecular dynamics simulations. Mol Phys. 2013;111:3345–3362.

25. Khalili-Araghi F, Ziervogel B, Gumbart JC, Roux B. Molecular dynamics simulations of membrane proteins under asymmetric ionic concentrations. J Gen Physiol. 2013;142:465–475.

26. Kutzner C, Grubmüller H, de Groot BL, Zachariae U. Computational electrophysiology: the molecular dynamics of ion channel permeation and selectivity in atomistic detail. Biophys J. 2011;101:809–817.

27. Gumbart J, Khalili-Araghi F, Sotomayor M, Roux B. Constant electric field simulations of the membrane potential illustrated with simple systems. Biochim Biophys Acta. 2012;1818:294–302.

28. Frenkel D, Smit B. Understanding molecular simulation: From algorithms to applications. 2nd ed. New York (NY): Academic Press; 2002.

29. Miyamoto S, Kollman PA. An analytical version of the SHAKE and RATTLE algorithm for rigid water models. J Comp Chem. 1992;13:952–962.

30. Tuckerman M, Berne BJ, Martyna GJ. Reversible multiple time scale molecular dynamics. J Chem Phys. 1992;97:1990–2001.

31. Jorgensen WL, Chandrasekhar J, Madura JD, Impey RW, Klein ML. Comparison of simple potential functions for simulating liquid water. J Chem Phys. 1983;79:926–935.

32. Joung IS, Cheatham III TE. Determination of alkali and halide monovalent ion parameters for use in explicitly solvated biomolecular simulations. J Phys Chem B. 2008;112:9020–9041.

33. Li P, Roberts BP, Chakravorty DK, Merz KM Jr. Rational design of particle mesh Ewald compatible Lennard-Jones parameters for +2 metal cations in explicit solvent. J Chem Theory Comput. 2013;9:2733–2748.

34. Wang J, Wolf RM, Caldwell JW, Kollman PA, Case DA. Development and testing of a general amber force field. J Comp Chem. 2004;25:1157–1174.

35. Wang J, Wang W, Kollman PA, Case DA. Automatic atom type and bond type perception in molecular mechanical calculations. J Mol Graphics Modell. 2006;25:247–260.

36. Jakalian A, Bush BL, Jack DB, Bayly CI. Fast, efficient generation of high-quality atomic charges. AM1-BCC model: I. method. J Comp Chem. 2000;21:132–146.

37. Jakalian A, Jack DB, Bayly CI. Fast, efficient generation of high-quality atomic charges. AM1-BCC model: II. parameterization and validation. J Comp Chem. 2002;23:1623–1641.

38. Phillips JC, Braun R, Wang W, Gumbart J, Tajkhorshid E, Villa E, Chipot C, Skeel RD, Kale L, Schulten K. Scalable molecular dynamics with NAMD. J Comp Chem. 2005;26:1781–1802.

39. Fink M, Lesage F, Duprat F, Heurteaux C, Reyes R, Fosset M, Lazdunski M. A neuronal two P domain K+ channel stimulated by arachidonic acid and polyunsaturated fatty acids. EMBO J. 1998;17:3297–3308.

40. Enyedi P, Czirják G. Molecular background of leak K+ currents: two-pore domain potassium channels. Physiol Rev. 2010;90:559–605.

41. Jensen MØ, Borhani DW, Lindorff-Larsen K, Maragakis P, Jogini V, Eastwood MP, Dror RO, Shaw DE. Principles of conduction and hydrophobic gating in K+ channels. Proc Natl Acad Sci USA. 2010;107:5833–5838.

42. Blin S, Soussia IB, Kim EJ, Brau F, Kang D, Lesage F, Bichet D. Mixing and matching TREK/TRAAK subunits generate heterodimeric K2P channels with unique properties. Proc Natl Acad Sci USA. 2016;113:4200–4205.

43. Bankura A, Carnevale V, Klein ML. Hydration structure of salt solutions from ab initio molecular dynamics. J Chem Phys. 2013;138:1–10.

44. Moldenhauer H, Díaz-Franulic I, González-Nilo F, Naranjo D. Effective pore size and radius of capture for K+ ions in K-channels. Sci Rep. 2016;6:1–5.

45. Brennecke JT, de Groot BL. Mechanism of mechanosensitive gating of the TREK-2 potassium channel. Biophys J. 2018;114:1336–1343.

46. Shaw DE, Grossman JP, Bank JA, Batson B, Butts JA, Chao JC, Deneroff MM, Dror RO, Even A, Fenton CH, et al. Anton 2: raising the bar for performance and programmability in a special-purpose molecular dynamics supercomputer. SC'14: Proceedings of the International Conference for High Performance Computing, Networking, Storage and Analysis; 2014 Nov 16–21; New Orleans, LA.

47. Wang Y, Harrison CB, Schulten K, McCammon JA. : Implementation of accelerated molecular dynamics in NAMD. Comput Sci Discov. 2011;4.1–10.

48. Adelman JL, Grabe M. Simulating current–voltage relationships for a narrow ion channel using the weighted ensemble method. J Chem Theory Comput. 2015;11:1907–1918.

List of Symbols, Abbreviations, and Acronyms

IC	intracellular cavity
K2P	two-pore domain K^+
MD	molecular dynamics
NAMD	Nanoscale Molecular Dynamics
NVT	constant volume–constant temperature
PDB	Protein Data Bank
PME	particle-mesh Ewald
POPC	(palmitoyl-oleoyl-phosphatidyl-choline)
RESPA	reference system propagator algorithm
SF	selectivity filter
TBI	traumatic brain injury
TIP3P	transferable intermolecular potential with 3 points
TRAAK	TWIK-related arachidonic acid-stimulated K^+ channel
VMD	Visual Molecular Dynamics

1 (PDF)	DEFENSE TECHNICAL INFORMATION CTR DTIC OCA
2 (PDF)	DIR ARL IMAL HRA RECORDS MGMT RDRL DCL TECH LIB
1 (PDF)	GOVT PRINTG OFC A MALHOTRA
2 (PDF)	ARL RDRL VT T CHANTAWANSRI RDRL VTM Y SLIOZBERG